CRYSTAL GROWTH & DESIGN

Article

Cite This: Cryst. Growth Des. 2019, 19, 6058−6066

pubs.acs.org/crystal

# Surface Induced Phenytoin Polymorph. 1. Full Structure Solution by Combining Grazing Incidence X-ray Diffraction and Crystal Structure Prediction

Doris E. Braun,[†] Arianna Rivalta,[‡] Andrea Giunchi,[‡] Natalia Bedoya-Martinez,[§] Benedikt Schrode,[∥,⊥] Elisabetta Venuti,[‡] Raffaele Guido Della Valle,[‡] and Oliver Werzer*[,⊥]

[†]Institute of Pharmacy, University of Innsbruck, Innrain 52c, 6020 Innsbruck, Austria

[‡]Department of Industrial Chemistry "Toso Montanari", University of Bologna, Viale Risorgimento 4, I-40136 Bologna, Italy

[§]Materials Center Leoben Forschung GmbH, Roseggerstraße 12, 8700 Leoben, Austria

[∥]Institute of Solid State Physics, NAWI Graz, Graz University of Technology, Petersgasse 16, 8010 Graz, Austria

[⊥]Institute of Pharmaceutical Science, Department of Pharmaceutical Technology, University of Graz, Univertitaetsplatz 1, 8010 Graz, Austria

Supporting Information

**ABSTRACT:** Understanding the behavior and properties of molecules assembled in thin layers requires knowledge of their crystalline packing. The drug phenytoin (5,5-diphenylhydantoin) is one of the compounds that can be grown as a surface induced polymorph. By using grazing incidence X-ray diffraction, the monoclinic unit cell of the new **form II** can be determined, but, due to crystal size and the low amount of data, a full solution using conventional structure solving strategies fails. In this work, the full solution has been obtained by combining computational structure generation and experimental results. The comparison between the bulk and the new surface induced phase reveals significant packing differences of the hydrogen-bonding network, which might be the reason for the faster dissolution of **form II** with respect to **form I**. The results are very satisfactory, and the method might be adapted for other systems, where, due to the limited amount of experimental data, one must rely on additional approaches to gain access to more detailed information to understand the solid-state behavior.

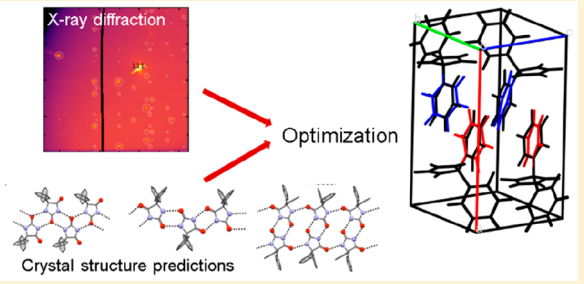


## INTRODUCTION

Polymorphism describes the capability of a defined chemical entity to adopt different solid-state arrangements.[1,2] In general, the selection of a polymorph for drug application is an important decision, as the physiochemical properties vary with the phase.[3] Accordingly, controlling polymorphism is a requirement in drug development to guarantee reproducible performances and is one of the crucial points for regulatory approval.

In addition to conventional bulk (solution) crystal form screening experiments, crystallization becomes more frequently investigated under more restricted environments like pores,[4] matrices,[5] or just at solid surfaces.[6] In any of those cases, the surface contact influences the nucleation. One reason might be the reduced local entropy of the system in the surface vicinity or the substrate−molecule interactions reducing the overall energy due to adhesion or other interactions. Eventually, this may determine a growth process distinct from the bulk case, resulting in a different crystal habit, a distinct crystal contact plane, and/or, maybe most importantly, in otherwise inaccessible polymorphs. The latter are often labeled as surface induced[7,8] or surface mediated phases[8] and might be a special case of heterogeneous crystallization. The extension of the new phases is often also limited in thickness, and these are then referred to as thin film phases; the organic semiconductor pentacene is one of the most prominent and widely studied examples of thin film polymorphism.[9] While such phases are often found, especially, when prepared within thin film facilitating spin coating or physical vacuum deposition, the reason for their occurrence is still not understood.

For active pharmaceutical ingredients (APIs) or simple drugs, thin film fabrication technologies have not yet been used extensively, as upscaling into mass production might require fabrication processes distinct from already established ones. For the sake of finding new polymorphs of drugs with the intention of reaching better solubility or overcoming patent issues, different film deposition techniques have been employed, including spin coating,[10−12] drop casting, inkjet

Received: July 2, 2019
Revised: September 15, 2019
Published: September 17, 2019




DOI: 10.1021/acs.cgd.9b00857
Cryst. Growth Des. 2019, 19, 6058−6066

printing, solution shearing,[13] dip coating, and vacuum deposition among others. The drug dissolution from such layers is often faster compared to bulk systems. On the one hand, this results from larger surface areas being present in the thin films[11] but also due to higher solubilities of the new forms.[12] These findings are of high importance as the low aqueous solubility of many new drug molecules under development requires improved strategies for successful medication development.

The characterization of a thin solid layer grown at a solid surface is challenging, and this is especially true if the structure, i.e., the assembly of the molecules within the unit cell, is unknown. To solve the structure of thin films from a few monolayers up to some hundreds of nanometers, grazing incidence X-ray diffraction (GIXD) is, besides electron diffraction, a method applicable. In short, diffraction from crystals gives reciprocal space information (peak positions and intensities). Peak positions determine the unit cell of the crystal, while the intensities provide structure information, i.e., the location of the atoms within the unit cell. Obtaining a direct solution is complicated due to the problem of lost phase information. Computer aided construction enables access to structural information either by direct or indirect methods. This approach works very well for most small molecular or macromolecular crystals, but, because of its statistical nature, many Bragg peaks are required for succeeding. Unfortunately, measuring GIXD or even electron diffraction provides often a limited number of Bragg reflections because of, for instance, too weak diffraction, small scattering volume, high aspect ratio or defects in the sample besides experimental damping resulting from temperature vibration (Debye−Waller like damping), or polarization of the X-ray beam. This restricts the usage of conventional structure solving approaches otherwise suitable for large single crystals.

In this work, we demonstrate that a full structure solution can be obtained from GIXD data, despite their limitations. To gain access to the structure of our sample of interest, phenytoin **form II**,[11,12,14] we combine the experimental findings with crystal structure prediction (CSP) calculations. CSP derives thermodynamically feasible molecular assemblies starting from the chemical structure only (Figure 1). The computationally

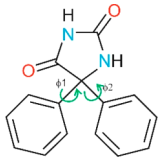


**Figure 1.** Molecular diagram of phenytoin. The intramolecular degrees of freedom (dihedral angles) optimized within the crystal energy minimizations (CrystalOptimizer, vide infra) are indicated with arrows.

generated structures can thus be used to produce theoretical diffraction patterns to compare to the experiments, finally allowing identification of the solution with the best match. This approach is demonstrated here in detail on the exemplary case of the recently found phenytoin thin film phase (**form II**). It is known that this phase[12] shows an improved drug release rate compared to the bulk polymorph counterpart, but the previous studies could not clarify why this difference exists. The knowledge of the structure gained in this work suggests that, in addition to differences in the crystal habit, also packing variations can explain the enhanced dissolution rate.

## EXPERIMENTAL METHODS

**Materials.** Pharmaceutical grade 5,5-diphenyl-2,4-imidazolidinedione (phenytoin) and tetrahydrofuran were purchased from Sigma-Aldrich (Germany) and used without further pretreatment or purification. Solutions of concentrations in the range of 0.1−10 mg/mL were prepared and stirred prior to use at room temperature.

Single crystal silicon wafers containing a layer of native oxide (Siegert Wafer, Germany) were used as substrates. Prior to use, the wafers were cut and cleaned subsequently in acetone, ethanol, and NaOH. Finally, they were rinsed with deionized water and blown dry under a nitrogen stream. Such substrates have isotropic surface properties. Thin films of phenytoin were fabricated by spin coating on top of the clean and dry substrates. For this, the substrate is mounted horizontally on a standard device and, after the deposition of 200 $\mu$L solution, the sample is put into rotation at a speed of 17 rps for 60 s to spread the liquid. After solvent removal, the film was crystallized. To maximize the amount of the new phase, the entire setup and the solution were placed inside an oven at 304 K. The optimization results are provided in the Supporting Information (section 7).

**X-ray Diffraction.** Grazing incidence X-ray diffraction (GIXD) was performed at the XRD1 beamline at the synchrotron ELETTRA (Trieste, Italy). In these experiments, the bending magnet radiation was monochromatized to a wavelength of 0.14 nm and guided through slits before interacting with the sample. The sample was mounted on a $\kappa$-goniometer and fixed with a custom-made vacuum holder which allowed in addition to level the sample surface with respect to the beam. A Pilatus 2 M detector (Dectris, Switzerland) collected the diffracted intensity. The blind detector areas due to detector construction are eliminated to a certain extent by taking images at slightly different detector positions. A self-written software, GIDVis,[15] was used to perform detector calibration, stitching, and overall data evaluation.

## COMPUTATIONAL METHODS

**Computational Exploration of the Crystal Energy Landscape.** Crystal structure prediction was carried out to identify the most stable hypothetical packing arrangements for phenytoin and to support the structure solution of **form II**. The CSP methodology employed, a multistep process, has been implemented successfully into experimental screening and characterization programs.[16,17]

The crystal energy landscape was explored using two different lowest energy conformations of the phenytoin molecule, obtained from Gaussian09[18] isolated molecule calculations, mapping the conformation potential energy surface (Supporting Information, Section 2). A total of 300 000 anhydrate structures were randomly generated in 48 space groups (Supporting Information, Section 3) using the program CrystalPredictor2.0.[19−21] Each crystal structure was relaxed to a local minimum in the intermolecular lattice energy, calculated with the FIT[22] *exp-6* repulsion-dispersion potential and with atomic charges fitted to the electrostatic potential around the PBE0/6-31G(d,p) charge density using the CHELPG scheme.[23]

All structures within 35 kJ mol$^{-1}$ of the lowest energy structure (2558 structures) were reminimized using DMACRYS[24] with a more realistic, distributed multipole model[25] for the electrostatic forces, derived using GDMA2[26] to analyze the PBE0/6-31G(d,p) charge density, resulting in 1727 unique structures. Thus, the intermolecular lattice energy includes now the highly directional electrostatic interactions arising from the lone pair and $\pi$ electrons.

To see the effects of minor changes in the molecular conformation, all structures within 23 kJ mol$^{-1}$ of the rigid body global minimum were further refined by simultaneous relaxation of the "flexible" internal degrees of freedom of the molecules (as defined in Figure 1) and the crystal structure. This was done by minimizing the lattice energy ($E_{latt}$), calculated as the sum of the intermolecular contribution ($U_{inter}$) and the conformational energy penalty paid for the distortion of the molecular geometry to improve the hydrogen bonding


DOI: 10.1021/acs.cgd.9b00857
Cryst. Growth Des. 2019, 19, 6058−6066

geometries. For each conformation considered in the minimization of $E_{latt}$, conformational energy penalties (taken as $\Delta E_{intra}$, with respect to the pyramidal global conformational energy minimum) and isolated molecule charge densities were computed at the PBE0/6-31G(d,p) level. Overall, 278 structures were minimized using the CrystalOptimizer database method.[27]

The most stable structures (91 structures) were then used as starting points for computationally time-consuming periodic electronic structure calculations. DFT-d calculations were carried out with the CASTEP v6.1. plane wave code[28] using the Perdew–Burke–Ernzerhof (PBE) generalized gradient approximation (GGA) exchange-correlation density functional[29] and ultrasoft pseudopotentials,[30] with the addition of the Tkatchenko and Scheffler (TS)[31] or Grimme 06 (D2)[32] semiempirical dispersion corrections. For more details, see section 1 of the Supporting Information. The crystallographic tool PLATON[33] was used in various steps to find the space group symmetry after unconstrained optimizations and to check for convergence to higher symmetries.

**Computed Structures for Forms I and II.** Among the many fully converged structures of crystalline phenytoin, possible candidate structures for **forms I** and **II** (bulk and SIP, respectively) were identified by matching computed and experimental lattice parameters and then further screened by comparing computed and experimental GIXD patterns. Since these structures were optimized within space group constraints, we must also verify that they are *local* minima of the potential energy surface, i.e., that their energy does not decrease on lowering the symmetry.

As a necessary mathematical condition for *local* stability of the lattice with respect to displacements of the atoms, the potential energy surface must in fact be convex around the stationary point reached by the optimization. Equivalently, the matrix formed by the second derivatives of the potential energy with respect to the atomic displacements must be *positive definite*; i.e., all the matrix eigenvalues must be positive.[34] A negative eigenvalue means that the system is at a saddle point and that the lattice is unstable with respect to displacements along the corresponding eigenvector.

The square root of the eigenvalues represents the vibrational frequencies of the lattice, which are spectroscopically observable. For this reason, calculated vibrational frequencies were used to verify that the candidate structures were stable (imaginary values indicate instability) and, as discussed in part 2 of this work, to experimentally confirm their correctness. Vibrational frequencies and eigenvectors for **form I** and **II** were computed by density functional theory (DFT) methods with the CASTEP v6.1 (without dispersion correction) and VASP software (Vienna Ab initio Simulation Package). The VASP calculations used the PBE exchange correlation functional in combination with projector-augmented wave (PAW) pseudopotentials.[35−37] The effects of van der Waals (vdW) interactions were included with the computationally efficient pairwise D3-BJ method by Grimme.[38] Whenever an imaginary frequency indicated that the stationary point was a saddle, nearby minima were easily reached by repeating the optimization after perturbing the system along the eigenvector of the mode with imaginary frequency.

**Crystal Explorer Calculations.** The pairwise energy contributions to the experimental structures were calculated using CrystalExplorer V17.[39−41] The optimized atomic positions (PBE-TS optimized structures) were used in all subsequent intermolecular interaction energy calculations. The model energies were calculated between all unique nearest neighbor molecular pairs. The model (termed CE-B3LYP) uses B3LYP/6-31G(d,p) molecular wave functions calculated by applying the molecular geometries extracted from the crystal structures. This approach employs electron densities of unperturbed monomers to obtain four separate energy components: electrostatic ($E_E$), polarization ($E_P$), dispersion ($E_D$), and exchange-repulsion ($E_R$). Each energy term is scaled independently to fit a large training set of B3LYP-D2/6-31G(d,p) counterpoise-corrected energies from both organic and inorganic crystals.[40]

## RESULTS AND DISCUSSION

**X-ray Diffraction.** Various reports demonstrated that phenytoin can assemble in two different polymorphs.[11,12] Spin coating, heating from the amorphous phase, or even solvent vapor annealing are shown to produce these phases. While these reports evidenced solely the presence of the bulk form (**form I**), the formation of solely the surface induced phase is hard to achieve. Nevertheless, optimizing the preparation procedure allowed obtaining samples of the phenytoin thin film phase with only a very little amount of concomitant **form I** (see Supporting Information). Using a spin coating process at the elevated temperature of 31 °C and a concentration of 1 mg/mL in THF was revealed to be the optimum condition for the **form II** (SIP) growth. Looking on the narrow parameter set for its formation, this means its occurrence delicately depends on the parameters, whereby the bulk form (**form I**) nucleates and grows over a much larger parameter range, even resulting in various habits or crystal textures.[42] Up to now, we only were able to achieve the **form II** when growth is performed in the vicinity of substrate and within thin films. This suggests that this phase is a surface induced thin film phase.

Many X-ray diffraction geometries exist which provide insight in the packing of molecules within thin films.[43] Information from net planes parallel to the substrate are derived from specular scans, typically referred to as $\theta/2\theta$ or $\theta/\theta$. Such measurements show that our optimized samples are highly textured, i.e., have one contact plane (see Supporting Information). Using grazing incidence X-ray diffraction, net planes not parallel to the surface become accessible, allowing the in-plane packing to be understood. GIXD measurements were performed by setting a defined angle of incidence of 1°. This damps the evanescent wave, but using high incident angles reduces the beam footprint at the sample enormously. Having a constant X-ray beam size, the photon flux onto the sample surface increases, while a smaller size/extension of the footprint then allows getting sufficient quality data; using a two-dimensional area detector on extended thin film samples results in severe peak smearing under grazing conditions. In addition, most pharmaceutical thin film samples consist of large crystals in the in-plane directions; thus a poor statistic often results when a measurement at only one azimuth is taken. For this reason, the sample requires rotation by 360° around its surface normal during data collection so that all diffraction spots are accessible making it a rotating GIXD experiment.[15] By doing this, an exemplary diffraction pattern as that of Figure 2 is obtained. This image represents a detailed view on the data, while in the Supporting Information (section 8) the entire pattern is shown, together with data from various other samples of different thickness.

Comparison of the Bragg peak positions with the already known structure of **form I** can be made but does not explain the measured peaks in Figure 2. For instance, a strong peak is located at about $q_p$ = 5 and $q_z$ = 13 nm$^{-1}$. Various peaks at constant $q_p$ = 10 nm$^{-1}$ or 14 nm$^{-1}$ are found at different $q_z$. As these spots are well-defined and not smeared, one can conclude that the mosaicity of the crystals is small. This fact is explained likely on account of the crystals growing in proximity to the substrate surface, i.e., where a two-dimensional confinement is taking place. The absence of rings or multiple peaks along a Debye ring also shows that all these surface-induced crystals contact the surface with the same


DOI: 10.1021/acs.cgd.9b00857
Cryst. Growth Des. 2019, 19, 6058−6066

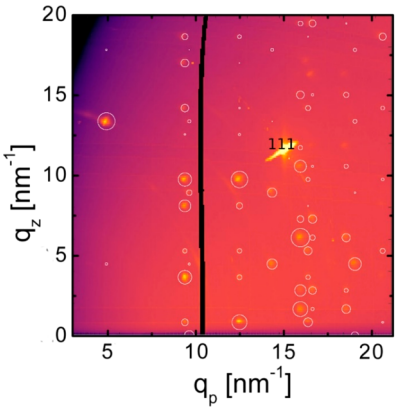


**Figure 2.** Grazing incidence X-ray diffraction pattern of phenytoin **form II**. Yellow spots are the high intensity Bragg peaks of phenytoin except the labeled peak at $q_p$ = 15 and $q_z$ = 12 nm$^{-1}$, which originates from the silicon substrate. The white circles represent calculated structure factors whereby the radius is directly proportional to its values.

$200_{SIP}$ net plane. The sample itself is polycrystalline with the individual crystals having azimuthal random arrangements which makes this structure a fiber textured one. In case of a single crystal or uniaxially alignment, the number of peaks would be low or even zero for an arbitrary measurement direction. The amount of diffraction information for the phenytoin sample here is only complete if the sample is rotated during measurement, thus collecting all information from such a two-dimensional powder. In a recent report,[12] many spots were missing due to the lack of proper rotation possibilities, which resulted in an incomplete information. Consequently, the previously determined unit cell was of low quality and cannot explain all peaks from the complete pattern shown here.

A unit cell of the new phenytoin form can be found, for example, by using the information on the peak positions and feeding this into a structure indexing software (DICVol04).[44] This software aims to find a unit cell just by knowing the experimentally determined *d*-spacings so that only the knowledge on the magnitude |**q**| of the scattering vector is needed, discarding any information on the position in $q_p$ or $q_z$. This approach yields a unit cell that explains the observed peak positions very well. The parameters extracted are given in Table 1 together with experimental literature data. Unlike **form I**, which is orthorhombic, the **form II** unit cell is monoclinic, with the monoclinic angle of 95.43°. Its unit cell axes *a* and *b* are shorter, resulting in a cell volume that is about 5% smaller than the volume of the bulk phase **form I**.

Knowing the unit cell dimensions gives some insight on the new phase, but no molecular or atomic arrangement can be derived. In a single crystal X-ray diffraction experiment, the next step would be extracting all the intensities of Bragg reflections accessible from the experiment (integration). In principle this can be done on GIXD data too. However, the data quality in comparison to single crystal results is still low, as the diffracting volume is small. Together with the decrease in intensity at large scattering vectors ($q$) due to polarization and area factor effects, this makes the extraction very uncertain. Furthermore, the number of quality peaks is low, about 20 in our case. Note that this does not allow using any of the standard procedures typically at hand for single crystal determination; as a rule of thumb the number of peaks required should be five times the number of atoms, which in our case would mean at least 100 high quality peaks. Therefore, we joined experimental and computational approaches to derive the packing information of **form II**.

**Computational Screening for Polymorphs.** The room temperature experimental anhydrate structure of **form I** was determined independently by four groups.[45−48] Interestingly, two different types of disorder have been described. The first two structure solutions (PHYDAN[45] and PHYDAN01[46]) report a small disorder in the two phenyl ring positions which can be related to the minimal intramolecular energy cost required for their rotation within a conformational energy well (Supporting Information, Section 2). The disorder described is in agreement with the observation seen in the PHYDAN03[48] structure; i.e., the phenyl rings show high thermal motion as derived from the atomic displacement parameters of the atoms. The structure solution PHYDAN02[47] shows directional disorder, i.e., oppositely directed H-bonded networks of the hydration moiety. Regardless of the H-bond orientation, the packing is maintained.

The PBE-TS and PBE-D2 lattice energy landscapes have several structures that are more stable in terms of lattice energies than the ordered experimental anhydrate **form I** (Figure 3a,b). The numbers assigned to the predicted

**Table 1. Experimental and Calculated Unit Cell Dimensions of Bulk and SIP Phenytoin, from the Literature and Obtained in This Work**

| structure | space group | $T^a$/K | *a*/Å | *b*/Å | *c*/Å | *β*/° | volume/Å$^3$ | CSD-refcode/structure ID |
|---|---|---|---|---|---|---|---|---|
| Form I (bulk) | | | | | | | | |
| exptl | $Pna2_1$ | RT | 6.230(1) | 13.581(1) | 15.532(2) | 90 | 1314.16 | PHYDAN[45] |
| exptl | $Pna2_1$ | RT | 6.228(1) | 13.568(1) | 15.520(2) | 90 | 1311.46 | PHYDAN01[46] |
| exptl | $Pna2_1$ | RT | 6.253(4) | 15.571(10) | 13.632(9) | 90 | 1327.29 | PHYDAN02[47] |
| exptl | $Pna2_1$ | RT | 6.237(4) | 15.552(10) | 13.614(12) | 90 | 1320.58 | PHYDAN03[48] |
| PBE-TS | $Pna2_1$ | 0 | 6.127 | 15.494 | 13.442 | 90 | 1275.92 | 780 |
| PBE-D2 | $Pna2_1$ | 0 | 6.160 | 15.453 | 13.226 | 90 | 1259.01 | 780 |
| Form II (SIP) | | | | | | | | |
| exptl | | 395 | 14.160 | 12.130 | 7.260 | 95.44 | 1241.37 | GIXD |
| PBE-TS | $P2_1/c$ | 0 | 14.102 | 12.119 | 7.187 | 99.25 | 1212.34 | 10 |
| PBE-D2 | $P2_1/c$ | 0 | 13.767 | 11.927 | 7.201 | 98.41 | 1169.64 | 10 |
| PBE-TS | *Pc* | 0 | 14.065 | 12.132 | 7.169 | 95.95 | 1216.61 | 10* |
| PBE-D2 | *Pc* | 0 | 13.796 | 11.939 | 7.212 | 95.41 | 1182.69 | 10* |

[a]RT − room temperature.



DOI: 10.1021/acs.cgd.9b00857
*Cryst. Growth Des.* 2019, 19, 6058−6066

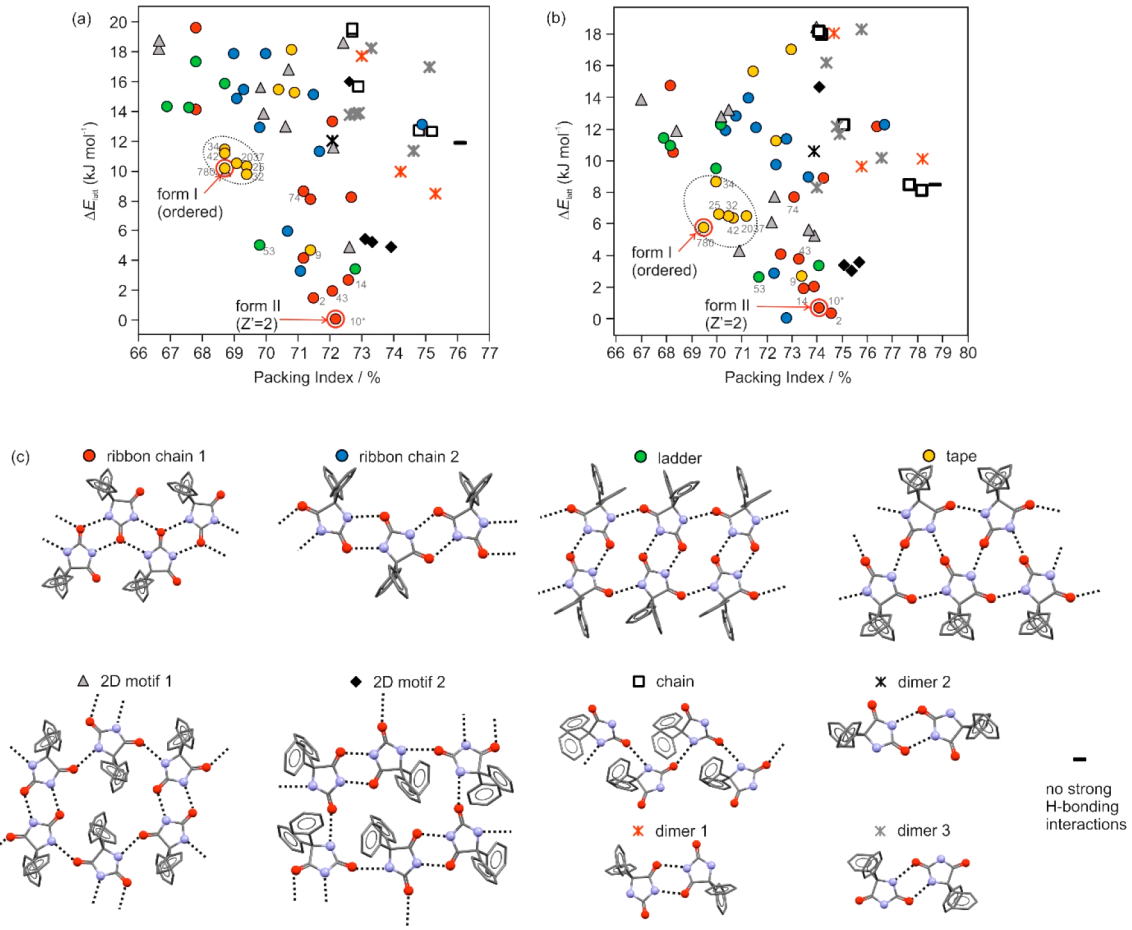


**Figure 3.** (a) PBE-TS and (b) PBE-D2 lattice energy landscapes for phenytoin, classified by H-bonding motif and packing mode (c). Each of the 67 symbols denotes a crystal structure, and each distinct symbol denotes a packing mode. Experimental structures are highlighted with red circles and arrows; structures labeled with structure ID number (Table S1 and S2 of the Supporting Information) show packing similarity with the experimental structures. The structures encircled with a dashed ellipsoid show high resemblance in packing and H-bonding motif with **form I**.

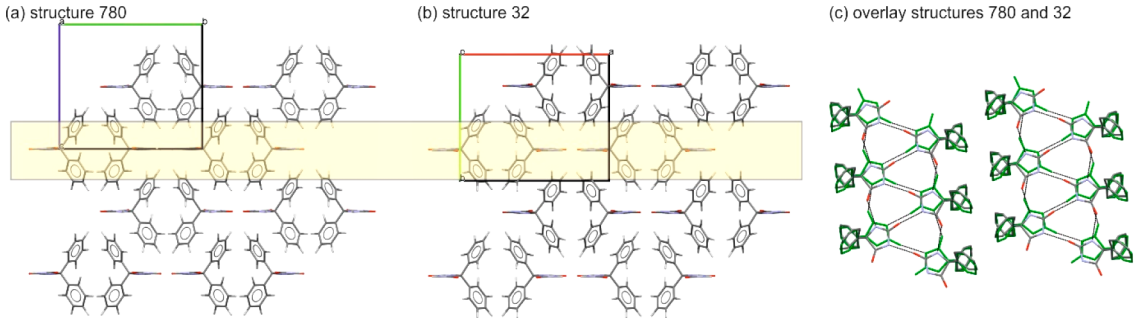


**Figure 4.** Packing diagrams of (a) structure 780 (ordered **form I**) and (b) structure 32, and a structure overlay of the regions highlighted in yellow in (a) and (b) is given in (c).

structures correspond to their initial order of ranking (CrystalPredictor).

The lowest-energy structures can be grouped according to hydrogen bonding motifs and packing modes. Five one-dimensional (1D: ribbon chains 1 and 2, ladder, tape, and chain), two 2D (motif 1 and 2), and three 0D (dimers) motifs were identified as recurring (Figure 3c). The tape **form I** motif was found 10 times among the lowest energy structures, albeit the specific packing was not found in the global minimum structure of either the PBE-TS (Figure 3a) or PBE-D2 (Figure 3b) lattice energy landscape. The lattice energy difference of the **form I** (structure 780) with respect to the global minimum PBE-TS ribbon chain 1 motif was calculated to be 10.2 kJ $mol^{-1}$ and with respect to the PBE-D2 ribbon chain 2 motif 5.7 kJ $mol^{-1}$. Such energy differences may be overestimated due to the lack of entropic contributions (disorder) in the lattice energy calculations, but present in the finite temperature **form I** structure. The close proximity of the tape structures of Figure 3 (similar lattice energies and similar packing indices), all differing only in the packing of the common and strongly H-bonded ladder motif, may be indicative of directional disorder. The combination of structures 780 (ordered **form I**, Figure 4a) and 32 (Figure 4b) reproduces the directional H-bonding disorder described in PHYDAN02[47] (Figure 4c). Furthermore,



DOI: 10.1021/acs.cgd.9b00857
*Cryst. Growth Des.* 2019, 19, 6058−6066

the lower packing indices of the tape motif structures, compared to the other structures, may be indicative of phenyl ring mobility, as seen in the experimental structures.

Independent of the chosen dispersion correction, the crystal energy landscapes suggest that phenytoin is polymorphic and that at very low temperature **form I** is not the most stable phase. The two ribbon chain motifs and the ladder motifs, as well as the two 2D packing motifs, are highly competitive with the **form I** H-bonding motif. In fact, the ribbon chain 1 packing motif dominates the lowest energy crystal structures in both the PBE-TS and PBE-D2 lattice energy landscapes, with the lowest ribbon chain 1 motifs showing 2D packing similarity.[49]

The PBE-D2 lattice energy landscape has a distinct packing, structure 8, as the global minimum. On the basis of the structure comparisons of the low energy structures, it can be concluded that phenytoin has numerous possibilities to form stable structures, which are based on distinct hydrogen bonding motifs. Indeed, the packing motifs of the yet unobserved forms can be found in the chemically related structure group of barbiturates.[50−52] Packing similarities within groups of structures sharing strong H-bonding interactions may be indicative of disorder, polytypism/domain structures[53] or concomitant polymorphism.[54] It should be noted that all computed structures are static, and the packings may allow phenyl ring rotations at finite temperature with minimal cost in intramolecular energy, but significant entropic stabilization.

**Computed Structures for Phases I and II.** As described in the Methods section, possible candidate structures for **forms I** and **II** were identified among the computed structures by matching computed lattice parameters and GIXD patterns against their experimental equivalents. Local stability of the lattice was then checked by computing the vibrational frequencies.

The ordered **form I** (bulk) was found to correspond to computed structure 780, space group $Pna2_1$, with four molecules per unit cell, all equivalent by symmetry ($Z = 4$, $Z' = 1$). The match between computed and experimental lattice parameters is good; the atomic coordinates are also well described, yielding $rmsd_{15}$ values[55] < 0.12 Å and < 0.18 Å for PBE-TS and PBE-D2 structures, respectively, compared to the experiments (see section 4 of the Supporting Information). The lattice is found to be stable since all vibrational frequencies are real and, as discussed in part 2 of this work, the experimental Raman spectra are satisfactorily described. All together, these excellent results indicate that the applied computational methods are valid and accurate.

For **form II** (SIP), the best match was initially found with computed structure 10, space group $P2_1/c$, with $Z = 4$ and $Z' = 1$. The agreement between computed and experimental lattice parameters was not perfect (Table 1), since the computed $\beta$ angle (99.25° for PBE-TS, 98.41° for PBE-D2) is larger than the experimental value (95.44°). Despite the slight discrepancy in the $\beta$ angle, the intensities of the experimental GIXD pattern were also reasonably reproduced with this initial results, showing that the crystal structure predicted is substantially correct. By computing the vibrational frequencies, however, we found an imaginary frequency (i.e., a negative eigenvalue), indicating that the $P2_1/c$ $Z' = 1$ structure corresponds to a saddle point rather than to a genuine energy minimum. The nearby minimum, therefore, was located by repeating the optimization after perturbing the system along the eigenvector of the mode with an imaginary frequency.

The optimized structure, labeled 10*, has space group $Pc$ ($Z' = 2$). The latter is slightly more stable than the original $P2_1/c$ saddle point (0.21 kJ $mol^{-1}$ using PBE-D2) and is geometrically extremely close, with an $rmsd_{15}$ value of 0.23 Å (Figure 5). Careful examination of the structures revealed that the

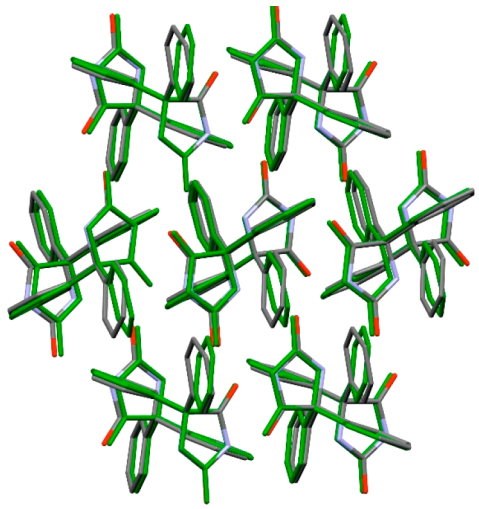

**Figure 5.** Overlay of the of the $P2_1/c$ ($Z' = 1$) saddle point structure (color coded in green) and the$Pc$ ($Z' = 2$) structures (coded in color).

transformation from the $P2_1/c$ saddle to the $Pc$ minimum involves small rotations of the phenyl groups in opposite directions, yielding two slightly different molecular conformations, not equivalent by symmetry ($Z = 4$, $Z' = 2$).

The lattice parameters computed for the $Pc$ structure 10* closely match the experimental values (Table 1). The computed $\beta$ angle, in particular, is now almost perfect (discrepancy 0.51° for PBE-TS, 0.03° for PBE-D2). The larger discrepancies for the computed $P2_1/c$ structures could be attributed to slight differences in the conformation of the molecules (Figure 5), which affect their packing with a more inclined unit cell. Most of the experimental GIXD pattern is reproduced by the $Pc$ structure 10* as shown in Figure 2 (structure factors are indicated by the ring size). Some more comparisons between diffractograms of experimental and computed structures are illustrated in the Supporting Information, section 7. It should be noted that a discrepancy of some peaks exists, which requires a further refinement which in single crystal or powder diffraction is regularly done to account for crystal dimensions, transparency/absorption, crystal defects, or molecular disorder.

Having now two likely structures, i.e., the $P2_1/c$ and $Pc$, a comparison with the experimental X-ray data show that actually only a small variation in the structure factors is noticeable, which due to the limited data quality in the GIXD experiment even does not allow us to pick the one over the other. In this particular case, we could find another criterion to justify the selection of the $Pc$ to being a better fitting choice than the $P2_1/c$, as it is discussed in part 2 of this work which is published separately. Raman spectroscopy was able to solve the puzzle. The vibrational spectra are excellent structural diagnostics since the lattice frequencies are extremely sensitive to the details of the crystal packing and in particular to the change in symmetry.[56] Using computed Raman spectra for the two predicted structures and comparisons with experimentally obtained vibrational spectra show that the $Pc$ agrees well, while



DOI: 10.1021/acs.cgd.9b00857
Cryst. Growth Des. 2019, 19, 6058−6066

those spectra computed for the $P2_1/c$ structure are unsatisfactory. We conclude that, because of the good match in lattice parameters, diffractogram and vibrational spectra, the computed *Pc* minimum correctly describes the **form II** crystal structure.

As a final comment to the found *Pc* structure 10*, it is necessary to add that, since from the saddle one may go down in two different directions (i.e., one may freely select the + or − sign for the perturbation), two distinct minima can be generated. However, the two optimized structures, which at first sight appeared to display opposite rotations of the phenyls, are actually identical but for a shift of the origin. Thus, the $P2_1/c$ saddle structure may be described as an average of two shifted, but otherwise identical, *Pc* minima (zero-point and thermal motion average over symmetrically equivalent lower symmetry structures, as seen for racemic naproxene[57]). The relationships among the various structures are illustrated in Figure 6.

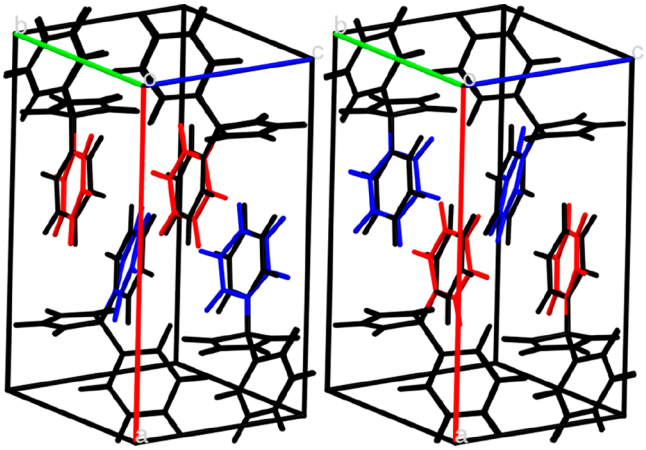

**Figure 6.** Molecular conformation and packing in the computed structures of **form II**. Overlay of structures $P2_1/c$ (black) and *Pc* (the two different molecular conformations are coded in color). The *Pc* structures in the two drawings (left and right) differ in the sign of the perturbation applied to the initial $P2_1/c$ structure, but are actually identical except for a shift of the origin. Their average corresponds to the $P2_1/c$ structure.

**Packing Considerations.** **Form I** and **form II** molecular conformations correspond to the same minimum of the isolated molecule potential surface (Supporting Information, section 2). At the same time, the two forms exhibit distinct H-bonding interactions (Figure 3c, ribbon chain 1 and tape) and show no packing similarities (Figure 7). The strong H-bonding interactions (N−H···O) account for 50% of the intermolecular interactions in **form I** and for ∼45% in **form II**. A direct comparison of the CE-B3LYP interaction energies present in **form I** and **form II** reveals that the N−H···O H-bonds, four in each polymorph, are of similar strengths (Table S4 of the Supporting Information). Close contacts, aromatic and C−H···$\pi$ interactions, contribute more to the lattice energy in **form II** than in **form I**, an observation which can be related to the fact that **form II** is more densely packed than **form I**, thus rationalizing the lower lattice energy calculated for **form II** at 0 K.

Besides the energy considerations, a relevant difference between the H-bonding networks of the two phases could be detected in **form I** having four adjacent H-bonded molecules,

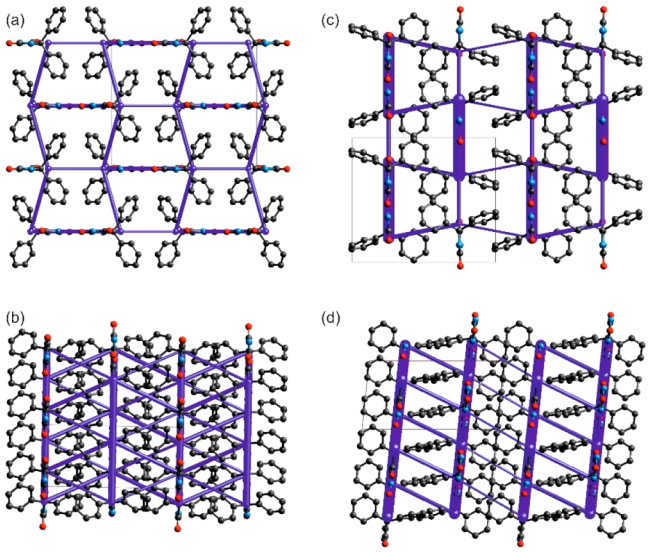


**Figure 7.** Energy frameworks (total intermolecular energy) for (a, b) **form I**, and (c, d) **form II** (*Pc*, $Z' = 2$). The energy scale factor is 80, and pairwise interaction energies with magnitudes smaller than 14 kJ $mol^{-1}$ have been omitted.

whereas **form II** has only two, but double H-bonded, with one H-bonding site at the oxygen even unmatched. While the variation in the energetics is hardly justifying any differences in the dissolution behavior, the steric arrangement of H-bonding network in phenytoin **form II** might be the cause of its increased aqueous dissolution rate.

## CONCLUSIONS

The evaluation of the structure within a thin film is challenging due to different reasons. By using a combination of CSP calculations with GIXD experiments and some help from Raman spectroscopy, the structure of phenytoin in its thin film form (**form II**) could be solved. The results suggest that the difference in the steric H-bonding network is likely the reason for the faster dissolution of the surface induced thin film form (**form II**) with respect to the **form I**, which is the bulk form. In general, the structure solving procedure employed here, with the assistance of CSP methods, allows for the use of limited experimental data to gain access to the packing arrangement of organic molecules. It can be expected that this may represent an optimal approach when dealing not only with GIXD data from thin films but could be extended to single crystal X-ray diffraction of poor data, neutron diffraction, or even electron diffraction, minimizing the requirement of high quality crystal growth.

## ASSOCIATED CONTENT

### Supporting Information

The Supporting Information is available free of charge on the ACS publication Web site. The Supporting Information is available free of charge on the ACS Publications website at DOI: 10.1021/acs.cgd.9b00857.

Computational section includes methodology computationally generated low-energy scans, computational generated low-energy structures, representation of the experimental structure, crystal explorer calculations; experimental section includes scattering geometries,



DOI: 10.1021/acs.cgd.9b00857
*Cryst. Growth Des.* 2019, 19, 6058−6066

maximizing **form II** within spin coating experiment, grazing incidence diffraction (PDF)

## AUTHOR INFORMATION


### Corresponding Author

*E-mail: oliver.werzer@uni-graz.at.

### ORCID

Doris E. Braun: 0000-0003-0503-4448
Arianna Rivalta: 0000-0002-0528-4044
Natalia Bedoya-Martinez: 0000-0001-9824-6129
Benedikt Schrode: 0000-0003-2013-9272
Elisabetta Venuti: 0000-0003-3493-7953
Oliver Werzer: 0000-0003-0732-4422


### Notes

The authors declare no competing financial interest.

## ACKNOWLEDGMENTS

The authors are grateful to Profs. C. C. Pantelides and C. S. Adjiman (Imperial College London) for the use of the CrystalPredictor and CrystalOptimizer programs and to Prof. S. L. Price (University College London) for the use of the DMACRYS program. CSP and CASTEP calculations have been performed using the HPC infrastructure LEO of the University of Innsbruck. O.W. and B.S. want to thank the FWF for financial support within the Project P 25541. Elettra synchrotron is acknowledged for providing beamtime at the XRD1 beamline, and the authors want to thank Luisa Barba and Nicola Demitri for their excellent support. N.B. gratefully acknowledges the financial support under the scope of the COMET program within the K2 Center "Integrated Computational Material, Process and Product Engineering (IC-MPPE)" (Project No 859480). This program is supported by the Austrian Federal Ministries for Transport, Innovation and Technology (BMVIT) and for Digital and Economic Affairs (BMDW), represented by the Austrian research funding association (FFG), and the federal states of Styria, Upper Austria and Tyrol.

## REFERENCES


(1) Bernstein, J. *Polymorphism in Molecular Crystals*; Clarendon Press: Oxford, 2002.
(2) Brittain, H. G. *Polymorphism in Pharmaceutical Solids*; Informa Healthcare: New York, London, 2009; Vol. *192*.
(3) Vippagunta, S. R.; Brittain, H. G.; Grant, D. J. W. Crystalline solids. *Adv. Drug Delivery Rev.* **2001**, *48*, 3.
(4) Diao, Y.; Myerson, A. S.; Hatton, T. A.; Trout, B. L. Surface Design for Controlled Crystallization: The Role of Surface Chemistry and Nanoscale Pores in Heterogeneous Nucleation. *Langmuir* **2011**, *27*, 5324.
(5) Kellner, T.; Ehmann, H. M. A.; Schrank, S.; Kunert, B.; Zimmer, A.; Roblegg, E.; et al. Crystallographic Textures and Morphologies of Solution Cast Ibuprofen Composite Films at Solid Surfaces. *Mol. Pharmaceutics* **2014**, *11*, 4084.
(6) Yazdanpanah, N.; Testa, C. J.; Perala, S. R. K.; Jensen, K. D.; Braatz, R. D.; Myerson, A. S.; et al. Continuous Heterogeneous Crystallization on Excipient Surfaces. *Cryst. Growth Des.* **2017**, *17*, 3321.
(7) Artusio, F.; Pisano, R. Surface-induced crystallization of pharmaceuticals and biopharmaceuticals: A review. *Int. J. Pharm.* **2018**, *547*, 190.
(8) Jones, A. O. F.; Chattopadhyay, B.; Geerts, Y. H.; Resel, R. Substrate-Induced and Thin-Film Phases: Polymorphism of Organic Materials on Surfaces. *Adv. Funct. Mater.* **2016**, *26*, 2233.
(9) Pachmajer, S.; Jones, A. O. F.; Truger, M.; Rothel, C.; Salzmann, I.; Werzer, O.; et al. Self-Limited Growth in Pentacene Thin Films. *ACS Appl. Mater. Interfaces* **2017**, *9*, 11977.
(10) Werzer, O.; Baumgartner, R.; Zawodzki, M.; Roblegg, E. Particular Film Formation of Phenytoin at Silica Surfaces. *Mol. Pharmaceutics* **2014**, *11*, 610.
(11) Rothel, C.; Ehmann, H. M. A.; Baumgartner, R.; Reischl, D.; Werzer, O. Alteration of texture and polymorph of phenytoin within thin films and its impact on dissolution. *CrystEngComm* **2016**, *18*, 588.
(12) Reischl, D.; Rothel, C.; Christian, P.; Roblegg, E.; Ehmann, H. M. A.; Salzmann, I.; et al. Surface-Induced Polymorphism as a Tool for Enhanced Dissolution: The Example of Phenytoin. *Cryst. Growth Des.* **2015**, *15*, 4687.
(13) Guthrie, S. M.; Smilgies, D. M.; Giri, G. Controlling Polymorphism in Pharmaceutical Compounds Using Solution Shearing. *Cryst. Growth Des.* **2018**, *18*, 602.
(14) Ehmann, H. M. A.; Baumgartner, R.; Kunert, B.; Zimmer, A.; Roblegg, E.; Werzer, O. Morphologies of Phenytoin Crystals at Silica Model Surfaces: Vapor Annealing versus Drop Casting. *J. Phys. Chem. C* **2014**, *118*, 12855.
(15) Schrode, B.; Pachmajer, S.; Dohr, M.; Röthel, C.; Domke, J.; Fritz, T.; et al. GIDVis – a Comprehensive Software Tool for Geometry-Independent Grazing Incidence X-Ray Diffraction Data Analysis and Pole Figure Calculations. *J. Appl. Crystallogr.* **2019**, *52*, 683–689.
(16) Braun, D. E.; Oberacher, H.; Arnhard, K.; Orlova, M.; Griesser, U. J. 4-Aminoquinaldine monohydrate polymorphism: prediction and impurity aided discovery of a difficult to access stable form. *CrystEngComm* **2016**, *18*, 4053.
(17) Braun, D. E.; Orlova, M.; Griesser, U. J. Creatine: Polymorphs Predicted and Found. *Cryst. Growth Des.* **2014**, *14*, 4895.
(18) Frisch, M. J.; Trucks, G. W.; Schlegel, H. B.; Scuseria, G. E.; Robb, J. M. A.; Cheeseman, R., et. al.; Gaussian Inc.: Wallingford, CT, 2009.
(19) Karamertzanis, P. G.; Pantelides, C. C. Ab initio crystal structure prediction-I. Rigid molecules. *J. Comput. Chem.* **2005**, *26*, 304.
(20) Karamertzanis, P. G.; Pantelides, C. C. Ab initio crystal structure prediction. II. Flexible molecules. *Mol. Phys.* **2007**, *105*, 273.
(21) Habgood, M.; Sugden, I. J.; Kazantsev, A. V.; Adjiman, C. S.; Pantelides, C. C. Efficient Handling of Molecular Flexibility in Ab Initio Generation of Crystal Structures. *J. Chem. Theory Comput.* **2015**, *11*, 1957.
(22) Coombes, D. S.; Price, S. L.; Willock, D. J.; Leslie, M. Role of Electrostatic Interactions in Determining the Crystal Structures of Polar Organic Molecules. A Distributed Multipole Study. *J. Phys. Chem.* **1996**, *100*, 7352.
(23) Breneman, C. M.; Wiberg, K. B. Determining Atom-Centered Monopoles From Molecular Electrostatic Potentials - The Need For High Sampling Density in Formamide Conformational-Analysis. *J. Comput. Chem.* **1990**, *11*, 361.
(24) Price, S. L.; Leslie, M.; Welch, G. W. A.; Habgood, M.; Price, L. S.; Karamertzanis, P. G.; et al. Modelling organic crystal structures using distributed multipole and polarizability-based model intermolecular potentials. *Phys. Chem. Chem. Phys.* **2010**, *12*, 8478.
(25) Stone, A. J. Distributed multipole analysis: Stability for large basis sets. *J. Chem. Theory Comput.* **2005**, *1*, 1128.
(26) Stone, A. J.; *GDMA: A Program for Performing Distributed Multipole Analysis of Wave Functions Calculated Using the Gaussian Program System*, version 2.2; University of Cambridge: Cambridge, United Kingdom, 2010.
(27) Kazantsev, A. V.; Karamertzanis, P. G.; Adjiman, C. S.; Pantelides, C. C. Efficient Handling of Molecular Flexibility in Lattice Energy Minimization of Organic Crystals. *J. Chem. Theory Comput.* **2011**, *7*, 1998.
(28) Clark, S. J.; Segall, M. D.; Pickard, C. J.; Hasnip, P. J.; Probert, M. J.; Refson, K.; et al. First principles methods using CASTEP. *Z. Kristallogr. - Cryst. Mater.* **2005**, *220*, 567.




DOI: 10.1021/acs.cgd.9b00857
*Cryst. Growth Des.* 2019, 19, 6058–6066

(29) Perdew, J. P.; Burke, K.; Ernzerhof, M. Generalized gradient approximation made simple. *Phys. Rev. Lett.* **1996**, *77*, 3865.
(30) Vanderbilt, D. Soft Self-Consistent Pseudopotentials in a Generalized Eigenvalue Formalism. *Phys. Rev. B: Condens. Matter Mater. Phys.* **1990**, *41*, 7892.
(31) Tkatchenko, A.; Scheffler, M. Accurate Molecular Van Der Waals Interactions from Ground-State Electron Density and Free-Atom Reference Data. *Phys. Rev. Lett.* **2009**, *102*, No. 073005/1.
(32) Grimme, S. Semiempirical GGA-type density functional constructed with a long-range dispersion correction. *J. Comput. Chem.* **2006**, *27*, 1787.
(33) Spek, A. L. Structure validation in chemical crystallography. *Acta Crystallogr., Sect. D: Biol. Crystallogr.* **2009**, *65*, 148.
(34) Born, M.; Huang, K. *Dynamical Theory of Crystal Lattices*; Oxford University Press: New York, 1954.
(35) Kresse, G.; Furthmuller, J. Efficient iterative schemes for ab initio total-energy calculations using a plane-wave basis set. *Phys. Rev. B: Condens. Matter Mater. Phys.* **1996**, *54*, 11169.
(36) Perdew; Chevary; Vosko; Jackson; Pederson; Singh.; et al. Erratum: Atoms, molecules, solids, and surfaces: Applications of the generalized gradient approximation for exchange and correlation. *Phys. Rev. B: Condens. Matter Mater. Phys.* **1993**, *48*, 4978.
(37) Kresse, G.; Hafner, J. Norm-conserving and ultrasoft pseudopotentials for first-row and transition elements. *J. Phys.: Condens. Matter* **1994**, *6*, 8245.
(38) Grimme, S.; Ehrlich, S.; Goerigk, L. Effect of the Damping Function in Dispersion Corrected Density Functional Theory. *J. Comput. Chem.* **2011**, *32*, 1456.
(39) Turner, M. J.; Thomas, S. P.; Shi, M. W.; Jayatilaka, D.; Spackman, M. A. Energy frameworks: insights into interaction anisotropy and the mechanical properties of molecular crystals. *Chem. Commun.* **2015**, *51*, 3735.
(40) Turner, M. J.; Grabowsky, S.; Jayatilaka, D.; Spackman, M. A. Accurate and Efficient Model Energies for Exploring Intermolecular Interactions in Molecular Crystals. *J. Phys. Chem. Lett.* **2014**, *5*, 4249.
(41) Mackenzie, C. F.; Spackman, P. R.; Jayatilaka, D.; Spackman, M. A. CrystalExplorer model energies and energy frameworks: extension to metal coordination compounds, organic salts, solvates and open-shell systems. *IUCrJ* **2017**, *4*, 575.
(42) Ehmann, H. M. A.; Baumgartner, R.; Reischl, D.; Roblegg, E.; Zimmer, A.; Resel, R.; et al. One Polymorph and Various Morphologies of Phenytoin at a Silica Surface Due to Preparation Kinetics. *Cryst. Growth Des.* **2015**, *15*, 326.
(43) Birkholz, M. *Thin Film Analysis by X-ray Scattering*; John Wiley & Sons, 2006.
(44) Boultif, A.; Louer, D. Powder pattern indexing with the dichotomy method. *J. Appl. Crystallogr.* **2004**, *37*, 724.
(45) Camerman, A.; Camerman, N. The stereochemical basis of anticonvulsant drug action. I. The crystal and molecular structure of diphenylhydantoin, a noncentrosymmetric structure solved by centric symbolic addition. *Acta Crystallogr., Sect. B: Struct. Crystallogr. Cryst. Chem.* **1971**, *27*, 2205.
(46) Chattopadhyay, T. K.; Palmer, R. A.; Lisgarten, J. N. X-ray structural and potential energy studies on zentropil (5,5-diphenyl-2,4-imidazolidine dione). *J. Crystallogr. Spectrosc. Res.* **1993**, *23*, 149.
(47) Moriyama, K.; Furuno, N.; Yamakawa, N. Crystal face identification by Raman microscopy for assessment of crystal habit of a drug. *Int. J. Pharm.* **2015**, *480*, 101.
(48) Kalaiarasi, C.; Sangeetha, P.; Pavan, M. S.; Kumaradhas, P. Crystal structure and theoretical charge density studies of dilantin molecule. *J. Mol. Struct.* **2018**, *1170*, 105.
(49) Gelbrich, T.; Threlfall, T. L.; Hursthouse, M. B. XPac dissimilarity parameters as quantitative descriptors of isostructurality: the case of fourteen 4,5′-substituted benzenesulfonamido-2-pyridines obtained by substituent interchange involving CF3/I/Br/Cl/F/Me/H. *CrystEngComm* **2012**, *14*, 5454.
(50) Gelbrich, T.; Braun, D. E.; Griesser, U. J. Specific energy contributions from competing hydrogen-bonded structures in six polymorphs of phenobarbital. *Chem. Cent. J.* **2016**, *10*, 8.
(51) Gelbrich, T.; Braun, D. E.; Oberparleiter, S.; Schottenberger, H.; Griesser, U. J. The hydrogen bonded structures of two 5-bromobarbituric acids and analysis of unequal C5-X and C5-X' bond lengths (X = X' = F, Cl, Br or Me) in 5,5-disubstituted barbituric acids. *Crystals* **2016**, *6*, 47.
(52) Gelbrich, T.; Rossi, D.; Hafele, C. A.; Griesser, U. J. Barbiturates with hydrogen-bonded layer and framework structures. *CrystEngComm* **2011**, *13*, 5502.
(53) Bond, A. D.; Boese, R.; Desiraju, G. R. On the polymorphism of aspirin: Crystalline aspirin as intergrowths of two "polymorphic" domains. *Angew. Chem., Int. Ed.* **2007**, *46*, 618.
(54) Braun, D. E.; Gelbrich, T.; Wurst, K.; Griesser, U. J. Computational and Experimental Characterization of Five Crystal Forms of Thymine: Packing Polymorphism, Polytypism/Disorder and Stoichiometric 0.8-Hydrate. *Cryst. Growth Des.* **2016**, *16*, 3480.
(55) Chisholm, J. A.; Motherwell, S. COMPACK: a program for identifying crystal structure similarity using distances. *J. Appl. Crystallogr.* **2005**, *38*, 228.
(56) Salzillo, T.; d'Agostino, S.; Rivalta, A.; Giunchi, A.; Brillante, A.; Della Valle, R. G.; et al. Structural, Spectroscopic, and Computational Characterization of the Concomitant Polymorphs of the Natural Semiconductor Indigo. *J. Phys. Chem. C* **2018**, *122*, 18422.
(57) Braun, D. E.; Ardid-Candel, M.; D'Oria, E.; Karamertzanis, P. G.; Arlin, J. B.; Florence, A. J.; et al. Racemic Naproxen: A Multidisciplinary Structural and Thermodynamic Comparison with the Enantiopure Form. *Cryst. Growth Des.* **2011**, *11*, 5659.


DOI: 10.1021/acs.cgd.9b00857
*Cryst. Growth Des.* 2019, 19, 6058−6066